

# Search for Quasar Pairs with *Gaia* Astrometric Data.

## I. Method and Candidates

Qihang Chen (陈启航)<sup>1,2</sup> , Liang Jing (荆亮)<sup>1,2</sup> , Xingyu Zhu (朱星宇)<sup>1,2</sup> , Yue Fang (方越)<sup>3</sup> ,  
Zizhao He (何紫朝)<sup>4</sup> , Zhuojun Deng (邓卓君)<sup>1,2</sup> , Cheng Xiang (向成)<sup>1,2</sup>, and Jianghua Wu (吴江华)<sup>1,2</sup> \* 

<sup>1</sup> School of Physics and Astronomy, Beijing Normal University, Beijing, 100875, China  
e-mail: jhwu@bnu.edu.cn

<sup>2</sup> Institute for Frontier in Astronomy and Astrophysics, Beijing Normal University, Beijing, 102206, China

<sup>3</sup> College of Intelligent Systems Science and Engineering, Hubei Minzu University, Enshi, Hubei, 445000, China

<sup>4</sup> Purple Mountain Observatory, Chinese Academy of Sciences, Nanjing, Jiangsu, 210023, China

Received XXXX, XXXX; accepted XXXX, XXXX

### ABSTRACT

Quasar pair, a special subclass of galaxy pair, is valuable in the investigation of quasar interaction, co-evolution, merger, and clustering, as well as the formation and evolution of galaxies and supermassive black holes. However, quasar pairs at kpc-scale are rare in the universe. The scarcity of available samples hindered the deeper exploration and statistics of these objects. In this work, we apply an astrometric method to systematically search for quasar candidates within a transverse distance of 100 kpc to known quasars in the Million Quasar Catalog. These candidates are *Gaia* sources with zero proper motion and zero parallax, which are the kinematic characteristics of extragalactic sources. Visual inspection of the sample was performed to remove the contamination of dense stellar fields and nearby galaxies. A total of 4,062 quasar pair candidates were isolated, with the median member separation, *Gaia* G-band magnitude, and redshift of 8.81", 20.49, and 1.59, respectively. Our catalog was compared with three major candidate quasar pair catalogs and identified 3,964 new quasar pair candidates previously uncataloged in the three catalogs. Extensive spectroscopic follow-up campaigns are being carried out to validate their astrophysical nature. Several interesting quasar pair candidates are highlighted and discussed. We also briefly discussed several techniques for improving the success rate of quasar pair selection.

**Key words.** methods: data analysis – methods: statistical – quasars: general – catalogs – astrometry

## 1. Introduction

Quasar is the extremely distant luminous nucleus of the active galaxy (AGN) and hosts a supermassive black hole (SMBH) surrounded by an accretion disk, from which the powerful radiation originates. There is usually an extensive dusty torus wrapping around the accretion disk, with the broad and narrow line regions (BLR and NLR) located on either side of the disk (e.g., Antonucci 1993; Urry & Padovani 1995; Netzer 2015). Since the discovery of quasars in the early 1960s (Schmidt 1963; Sandage 1965), numerous surveys have discovered approximately one million such objects (the Million Quasar Catalog, Fleisch 2023). The most recently released DESI DR1 even has reported 1.65 million quasars, substantially expanding the known quasar population (DESI Collaboration et al. 2025).

If two quasars or galaxies encounter and interact, they may form a type of system known as “**quasar pair**”, which is quite a tiny fraction of the quasar population. Observationally, quasar pairs exhibit typical separations of less than several arcseconds and nearly identical redshifts, corresponding to sub-Mpc transverse physical distances. According to De Rosa et al. (2019), quasar pairs can be classified into two subclasses, **dual quasar** and **binary quasar**, based on the transverse distances between pair members. The dual quasar is defined as an interacting galaxy system containing two active nuclei that are not mutually gravitationally bound. The transverse distance between the

two quasars ranges from  $\sim 1$  pc to  $\sim 100$  kpc. The binary quasar refers to two quasars that are gravitationally bound and forming a Keplerian binary. The two quasars are separated by pc  $\sim$  sub-pc transverse distance. Quasar pairs are natural results of the hierarchical evolution of galaxies. They are important laboratories to study the quasar interaction, co-evolution, environment overdensity, clustering, large-scale structure, the growth of SMBHs, and the formation and evolution of galaxies in extreme environments or early universe (e.g., Begelman et al. 1980; Impey 1998; Yu 2002; Hennawi et al. 2006; Myers et al. 2008; Liu et al. 2011; Shen et al. 2010, 2023b; Merritt 2013; Sandrinelli et al. 2014, 2018; Hou et al. 2020; An et al. 2022; Xu et al. 2024; Wang et al. 2023b). They are also potential origins of nanohertz gravitational waves (nHz-GWs) in the early universe (Kelley et al. 2019; Chen et al. 2020; Shen et al. 2023a).

However, the rarity of confirmed quasar pairs inhibited deep exploration and statistical investigations. According to recent statistical work, only  $\sim 160$  quasar pairs with a transverse distance of less than 100 kpc are publicly confirmed to date (The Big MAC DR1, Pfeifle et al. 2024). It is therefore important to search for more of them. The search for quasar pairs can be dated back to Stockton (1972) and Wampler et al. (1973). However, their discoveries are not true quasar pairs but projected cases. The first populations of quasar pairs were discovered by some optical and radio surveys (e.g., Bolton et al. 1976; Meylan et al. 1987; Djorgovski et al. 1987; Muñoz et al. 1998). With the successive conduction of large-scale imaging sky sur-

\* Corresponding authors: jhwu@bnu.edu.cn

veys like SDSS (York et al. 2000), WISE (Wright et al. 2010), Pan-STARRS (Chambers et al. 2016), and recent DESI Legacy Imaging Surveys (DESI-LS, Dey et al. 2019), a significant number of quasar pairs and their candidates have been discovered by utilizing color-based method and spectroscopic follow-up (e.g., Hennawi et al. 2010; Green et al. 2010; Chen 2021). Several tens of quasar pairs have also been discovered as by-products of the search for strongly lensed quasars (e.g., Yue et al. 2023; Dawes et al. 2023; He et al. 2025), for example, the “Binary Quasar” sub-catalog compiled from the *Gravitationally lensed quasars in Gaia* project<sup>1</sup> (GLQG, Lemon et al. 2017). Furthermore, a recently proposed image decomposition method has also discovered a few quasar pairs (e.g., Silverman et al. 2020; Tang et al. 2021). In addition, several indirect methods have been used to search for quasar pairs with various characteristics, such as periodic variability (Sillanpää et al. 1988; Graham et al. 2015b,a; Liao et al. 2021; Davis et al. 2024), radial velocity drift (Guo et al. 2019; Zheng et al. 2023), double-peaked emission lines (Zhou et al. 2004; Boroson & Lauer 2009; Tang & Grindlay 2009; Shen & Loeb 2010; Kim et al. 2020a,b; Zheng et al. 2024), asymmetric emission line profiles (Eracleous et al. 2012a), continuum anomalies (Yan et al. 2015), as well as the observations of binary active cores in radio or X-ray images (Liu et al. 2003; Komossa et al. 2003). However, these indirect methods are not entirely reliable. The periodic variability induced by orbital motion can be easily imitated by the intrinsic irregular variability of the quasars (Charisi et al. 2016). Accretion disks can also produce double-peaked emission line profiles (Eracleous et al. 1997, 2012b), and some double-peaked narrow-line objects have been confirmed to be single sources (Foord et al. 2020). A single source can also produce velocity drift, double-peaked profile, and change of the profile of emission lines (Du & Wang 2023). The color- or SED-based method also has limitations, as the quasar region in the color-color diagram is heavily contaminated by some specific spectral types of stars (Ross et al. 2012; Wu et al. 2012; Yèche et al. 2020). A combination of optical imaging and spectroscopic surveys seems to be a promising and efficient search for quasar pairs.

The astrometric search for quasars is one of the most remarkable and promising methods. Quasars behave as apparently stationary (zero proper motion and zero parallax) objects in the sky because of their enormous distance from us. Quasar selection with the astrometric method can be traced back to Koo et al. (1986). They separated quasars from white dwarfs with the assistance of a proper motion criterion and demonstrated the power of the astrometric method. To make efficient and unbiased searches for quasars, several efforts pay attention to the astrometric method (e.g., Shu et al. 2019; Wu et al. 2023). Heintz et al. (2015, 2018, 2020) applied a pure astrometric method to select quasars and derived a conservative selection efficiency of  $\sim 75\%$ , indicating great success on quasar selection with astrometry. Lemon et al. (2019) presented a stricter criterion of proper motion significance (PMSIG) to assist the search for lensed quasars. Similarly, a probability-based zero proper motion method ( $f_{PMO}$ ), which is more complete mathematically than PMSIG, was proposed to help select quasar candidates behind the Galactic plane (GPQ, Fu et al. 2021). These efforts indicate the powerful capability of astrometry on quasar selection.

For the quasar pair search, the joint significance of the total proper motion  $\chi^2$  successfully selected some quasar pairs with quite small member separations around  $1''$  (Souchay et al.

2022; Makarov & Secrest 2022). On the other hand, some novel methods that utilize anomalous astrometry (Makarov et al. 2012; Makarov & Secrest 2023; Wu et al. 2022; Ji et al. 2023a), optical flickering or photometric centroid shift (e.g., Liu 2015, 2016), *Gaia* multi-peak (GMP, Mannucci et al. 2022, 2023; Ciurlo et al. 2023; Scialpi et al. 2024; Wu et al. 2024) and astrometric jitter/disturbance techniques (*Vastrometry*, see e.g., Shen et al. 2019, 2021; Hwang et al. 2020; Chen et al. 2022, 2023b; Wang et al. 2023a; Uppal et al. 2024; Schwartzman et al. 2024, for details of both the optical *Varstrometry for Off-nucleus and Dual sub-Kpc AGN* or VODKA, and radio *Varstrometry for Dual AGN using Radio interferometry* or VaDAR projects) have also discovered several tens of spatially unresolved or marginally resolved dual AGNs/quasars or SMBHs that separated by less than  $1''$  (from sub-kpc to a few kpc), opening up new avenues to in-depth exploration of the “final parsec problem” (e.g., Milosavljević & Merritt 2001; Merritt & Milosavljević 2005; Zhang 2023; Bromley et al. 2024; Koo et al. 2024). A serendipitously discovered quasar pair at  $z = 1.76$  and with member separation of  $8.76''$  indicates that the selection of point sources without significant proper motion next to known quasars could be an effective way to search for quasar pairs (Altamura et al. 2020).

Referring to the probability-based astrometric criteria from Fu et al. (2021) and inspired by Altamura et al. (2020), we initiated a project for a systematic search for new quasars near known quasars to find new quasar pairs with a combination of *Gaia* astrometric data and the Million Quasar Catalog (MQC). The paper is organized as follows. The data exploited in this work, method details, and the derived candidates are introduced in Sec. 2. The basic statistical properties of the quasar pair candidates, the comparative advantages of our sample over three major candidate quasar pair catalogs, and several interesting candidates are described in Sec. 3. The conclusion and discussion on quasar pair selection improvement are given in Sec. 4. Throughout this paper, we adopt a flat  $\Lambda$ CDM cosmology with  $\Omega_\Lambda = 0.7$ ,  $\Omega_M = 0.3$ , and  $H_0 = 70 \text{ km} \cdot \text{s}^{-1} \cdot \text{Mpc}^{-1}$ .

## 2. Data and Method

The catalogs used in this work include version 8.0 of MQC and *Gaia* Data Release 3 (*Gaia* DR3). The imaging data of DESI-LS and Pan-STARRS are used to visually inspect and classify the astrometrically selected quasar pair candidates.

### 2.1. Data

The MQC is extended from the Half Million Quasar Catalog (Flesch 2015). The sources included can be traced back to the first catalog release (version 0.1) on 22 April 2009. After 14 years of continuous expansion and the addition of quasar samples confirmed from large numbers of multi-band photometric and spectroscopic surveys, the final version 8.0 of the MQC (hereafter MQCv8)<sup>2</sup> was published on 2 August 2023 (Flesch 2023). The MQCv8 contains 1,021,800 quasars and high-probability candidates, of which 60.7% show *Gaia* DR3 astrometry. It provides a sufficient basis to search for quasar pairs systematically.

*Gaia* is a powerful space astrometric satellite launched by the European Space Agency (ESA) in December 2013. The mission is for a space-based, astrometric, and photometric all-sky survey at optical wavelengths, providing more than one billion ac-

<sup>1</sup> <https://research.ast.cam.ac.uk/lensedquasars/binaries.html>

<sup>2</sup> MILLIQUAS v8.0 (2023) update, <https://heasarc.gsfc.nasa.gov/W3Browse/all/milliquas.html>

curate measurements of astrometric parameters for a variety of objects (de Bruijne 2012; Gaia Collaboration et al. 2016). Under the *Gaia*'s unprecedented measurement accuracy of a few  $\mu\text{as}$ , extragalactic sources and objects in the Milky Way can be discriminated effectively by astrometric parameters like proper motion and parallax. *Gaia* published its DR3 on 2022 Jun 13th (Gaia Collaboration et al. 2022), which contains 1.8 billion astrometric objects and 1.5 billion sources with measured proper motions and parallaxes, of which the accuracy is as high as 0.001 mas/yr.

## 2.2. Method

Based on the combination of the latest MQC and the most enormous astrometric database, searching for extragalactic sources with proper motion and parallax consistent with zero near the spectroscopically confirmed quasars has immense advantages in the catalog volume, coordinate accuracy, and the quasar selection bias. The following three major steps are executed to obtain the quasar pair candidates:

- 1) Cross-match between MQCv8 and *Gaia* DR3;
- 2) Astrometric filter on the cross-matched catalog;
- 3) Visual inspection of the astrometrically selected pair candidates.

### 2.2.1. cross-match

The catalog cross-matching tool, TOPCAT (Taylor 2005), was employed to carry out the first step of our method. To start with, quasars in MQCv8 were searched in the SIMBAD database<sup>3</sup> (Wenger et al. 2000) using a  $1''$  radius to update their redshift. Then the quasars with  $z \geq 0.5$  were selected as the base sample, which includes 908,990 quasars. To exclude the quasars with imprecise radio or X-band positions, we cross matched the 908,990 quasars with *Gaia* DR3 using a search radius of  $1''$ . The *Gaia* match closest to the position of the quasar was considered as its *Gaia* counterpart. This yields a *Gaia* optical quasar sample, which consists of 582,725 quasars with *Gaia* detections.

Based on the updated redshift, the angular separation corresponding to a transverse distance of 100 kpc to each optical quasar was calculated under the flat  $\Lambda$ CDM cosmology. These separations were used to perform the cross-match of *Gaia* DR3 sources to the optical quasars with *Gaia* positions. A total of 105,971 *Gaia* sources within 100 kpc to the MQCv8 quasars were selected to constitute a preliminary catalog, which is marked as 100kpcCAT. Then, the 100kpcCAT was searched again in SIMBAD within a radius of  $1''$  to exclude those spectroscopically confirmed sources. Finally, a sample of 85,913 sources with proper motion and parallax measurements but without redshift was isolated as the input sample of the next step of the astrometric filter. For convenience, we name this sample as *astrometricCAT*.

### 2.2.2. astrometric filter

To support the astrometric filter, two reference samples of SDSS DR18 quasars and stars were retrieved from SDSS Science Archive Server<sup>4</sup> (SAS) and cross matched with *Gaia* DR3 to obtain their astrometric measurements. To regulate the quantity and quality of reference samples, 100,000 quasars and 100,000

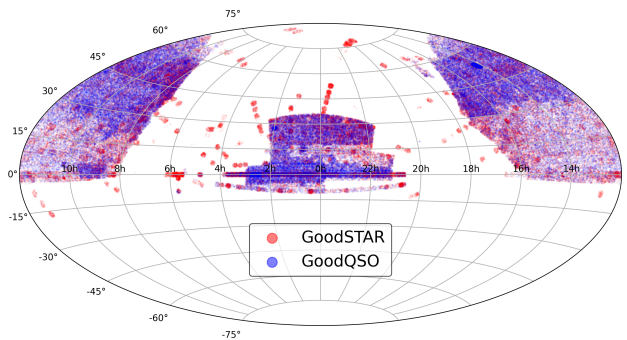


**Fig. 1.** The Hammer-Aitoff equatorial projection of GoodQSO (blue) and GoodSTAR (red).

stars were selected randomly according to their equatorial coordinates. The distributions of these quasars and stars in equatorial coordinates are displayed in Figure 1. The equal volume of the two samples ensures an unbiased astrometric filter. All the sources in the two samples have both proper motion and parallax measurements in *Gaia*, and their *Gaia* G-band magnitudes are in the range of  $17 \leq G \leq 21$ . The setting of this magnitude range is to exclude extremely faint sources that may have poor astrometric accuracy, and to ensure consistency with the predominantly faint nature of the *astrometricCAT* (with the median *Gaia* G-band magnitude of 19.32). The two reference samples are denoted as GoodQSO and GoodSTAR hereafter. They are the keys to the astrometric filter.

Utilizing several astrometric measurements provided by *Gaia* DR3, a couple of astrometric criteria are proposed to select extragalactic candidates efficiently. The astrometric measurements include the total proper motion (PM), parallax (Plx), and their uncertainties (PM\_err and Plx\_err). Following Fu et al. (2021), the probability densities of zero proper motion and zero parallax are employed to set the astrometric criteria. And following Heintz et al. (2018, 2020), the SNRs of proper motion and parallax are invoked for a comparison.

Equation 10 in Fu et al. (2021) defines the probability density of zero proper motion of a *Gaia* DR2 source. Here, this work disregards the zero-point drift  $\sigma_s$  (i.e., the systematic error) and the multiplicative factor  $k$ , and defines the probability density of zero proper motion of a *Gaia* DR3 source as:

$$f_{0pm} = \frac{1}{\sqrt{2\pi}\sigma_{pm}} \cdot \exp\left[-\frac{(pm - \mu_{pm})^2}{2\sigma_{pm}^2}\right], \quad (1)$$

where  $pm$  and  $\sigma_{pm}$  represent the proper motion and its uncertainty, respectively, while  $\mu_{pm}$  denotes the global systematic uncertainty of proper motion. We assumed it to be zero for simplicity.

Considering that the parallax of the Galactic stars is generally significant, whereas extragalactic sources exhibit almost zero parallaxes, an additional criterion, the probability density of zero parallaxes, is introduced by us to constrain the kinematic characteristics of the sources further and to eliminate the Galactic stellar contaminants with coincidental zero proper motion. Similarly, the probability density of zero parallax is defined as:

$$f_{0plx} = \frac{1}{\sqrt{2\pi}\sigma_{plx}} \cdot \exp\left[-\frac{(plx - \mu_{plx})^2}{2\sigma_{plx}^2}\right], \quad (2)$$

where  $plx$  and  $\sigma_{plx}$  represent the parallax and its uncertainty, respectively, while  $\mu_{plx}$  denotes the global systematic uncertainty of parallax, which is also assumed to be zero for simplicity.

<sup>3</sup> <http://simbad.cds.unistra.fr/simbad/>

<sup>4</sup> <https://dr18.sdss.org/optical/spectrum/search>

The  $f_{0pm}$  and  $f_{0plx}$  are calculated for all sources in the GoodQSO and GoodSTAR and the logarithm of them ( $\log f_{0pm}$  and  $\log f_{0plx}$ ) are adopted for better visualization. The *left panel* in Figure 2 displays the  $\log f_{0pm}$  v.s.  $\log f_{0plx}$  distribution of the GoodQSO and GoodSTAR. After iterative attempts on the thresholds of criteria, we determined a couple of appropriate astrometric criteria that impose joint constraints on the proper motion and parallax:

- (1)  $\log f_{0pm} \geq -2$ ;
- (2)  $\log f_{0plx} \geq -2$ .

Then, following Heintz et al. (2020), the SNRs of proper motion and parallax for GoodQSO and GoodSTAR were also calculated, where  $\text{SNR}_{(pm)} = |\text{PM}/\text{PM\_err}| \leq 3$  and  $\text{SNR}_{(plx)} = |\text{Plx}/\text{Plx\_err}| \leq 3$  were set as the optimal criteria to isolate quasars from stars (*right panel* in Figure 2). By comparing the probability-based astrometric criteria with the SNR-based ones, we found that the purity of the quasar selection was 89.2% and 88.5%, respectively, while the completeness was 97.3% and 98.0%. This indicates that the efficiency of the two techniques is roughly equivalent. We adopted the probability-based astrometric filtering to isolate our quasar pair candidates. The two criteria are stricter than those of Fu et al. (2021), which ensures that we focus on the purity of quasar selection again. The filtering isolated a sample of 5,851 quasar candidates, denoted as MGQPCpreCAT, from the astrometricCAT.

### 2.2.3. visual inspection

The astrometric filtering only isolates extragalactic sources and cannot distinguish between galaxies and quasars. So the MGQPCpreCAT still requires morphological classification to exclude extended sources. On the other hand, no masking or special treatment was applied to the sky coverage of the Galactic plane, stellar clusters, or nearby galaxies during the cross-match and astrometric filtering. The contamination of these dense stellar fields cannot be overlooked. Therefore, we performed a visual inspection on the MGQPCpreCAT sources to remove this contamination. Limited by our available spectroscopic observation opportunities, the first stage (STAGE-I) of the visual inspection and spectroscopic follow-up focuses on 4,168 MGQPCpreCAT sources in the sky coverage of  $\text{Dec} \geq -30^\circ$ , which is the Pan-STARRS footprint.

The pseudo-color images of DESI-LS DR10<sup>5</sup> were plotted for the MGQPCpreCAT sources to assist the visual inspection. Although DESI-LS DR10 has covered nearly the entire sky, it lacks imaging data along the Galactic plane. Therefore, the Pan-STARRS imaging data<sup>6</sup> were used to supplement the DESI-LS images in the areas with  $\text{Dec} \geq -30^\circ$  where DESI-LS DR10 lacks imaging, or the imaging quality is poor. The pseudo-color images from DESI-LS DR10 are composed of the g, r, i, and z-bands data, but in some regions, not all four bands are available. When there are fewer than three bands of data in certain regions, the pseudo-color images are composed of the Pan-STARRS g, r, i, z, and y-bands data.

Visual inspection allows for the relatively easy and quick exclusion of dense stellar fields in the Galactic plane and most nearby galaxies. It has removed 106 such cases. Figure 3 shows examples of them in the MGQPCpreCAT. A total of **4,062** plausible quasar pair candidates are selected in the  $\text{Dec} \geq -30^\circ$

region. We designate them as ‘‘MGQPCs’’, which stands for ‘‘Quasar Pair Candidates derived from the cross-match of MQC and Gaia’’. The flowchart of the MGQPCs selection is shown in Figure 4.

## 3. Overview of the MGQPC catalog

The basic statistical features of the final sample of quasar pair candidates (MGQPCs) and the advantages of the MGQPC catalog are described and validated here. Several fascinating pair systems are also described in this section.

### 3.1. Basic features of MGQPCs

The comparison of the equatorial projection of the MGQPCpreCAT and the visually selected MGQPCs is displayed in Figure 5. Most MGQPCs are distributed in the SDSS footprint, and the Declination cut excluded the heaviest extragalactic stellar contamination of the Large and Small Magellanic Clouds. Figure 6 plots the MGQPCs’ *Gaia* G-band magnitude histogram (*top panel*) and distribution of the separation v.s. redshift (*bottom panel*). The redshifts are invoked from the known member quasars. The MGQPC catalog is dominated by faint sources and moderately large separations, with the median G-band magnitude and separation of  $\sim 20.5$  and  $\sim 8.8''$ , respectively. The rapid decrease in the G-band magnitude histogram at  $G \gtrsim 20.9$  mag is due to the bad *Gaia* measurements. The number of MGQPCs decreases with increasing redshift and decreasing separation. Examples of MGQPCs are displayed in Figure 7. A description of the primary columns in the MGQPC catalog is shown in Table 1.

### 3.2. Advantages of the MGQPC catalog

To clarify the sample advantages of the MGQPCs, three recently published and relatively larger candidate quasar pair catalogs or catalogs containing a substantial number of quasar pair candidates are introduced here for comparison with the MGQPC catalog at three aspects (member separation, *Gaia* G-band magnitude, and redshift). The three catalogs are briefly described as follows:

1. The first one is a catalog of 436 multiply lensed and binary quasar candidates (875 individual sources) obtained by Dawes et al. (2023, hereafter Dawes23) from the DESI-LS catalog by applying an autocorrelation algorithm.
2. The second is a catalog of lensed quasar and quasar pair candidates, comprising 971 systems (1,977 individual sources), compiled by He et al. (2023, hereafter He23) based on the DESI-LS catalog and color similarity method.
3. The last is a golden sample of 1,867 dual quasar candidates derived by Wu et al. (2024, hereafter Wu24) using the GMP technique.

All these catalogs were recompiled here by cross matching SIMBAD to update the redshifts and remove the newly confirmed pairs, and by cross matching *Gaia* DR3 to retrieve the *Gaia* coordinates and G-band magnitudes of their members. The member separations were calculated according to the member coordinates. Note that the candidates in Wu24 are not pairs of *Gaia* sources but single sources with possible multiple components, and most of them have spectroscopic or photometric redshifts, with only 298 candidates lacking redshift. After our re-compilation, there are 435, 994, and 1,867 candidate quasar pairs

<sup>5</sup> <https://www.legacysurvey.org/viewer>

<sup>6</sup> <https://pslimages.stsci.edu/cgi-bin/ps1cutouts>

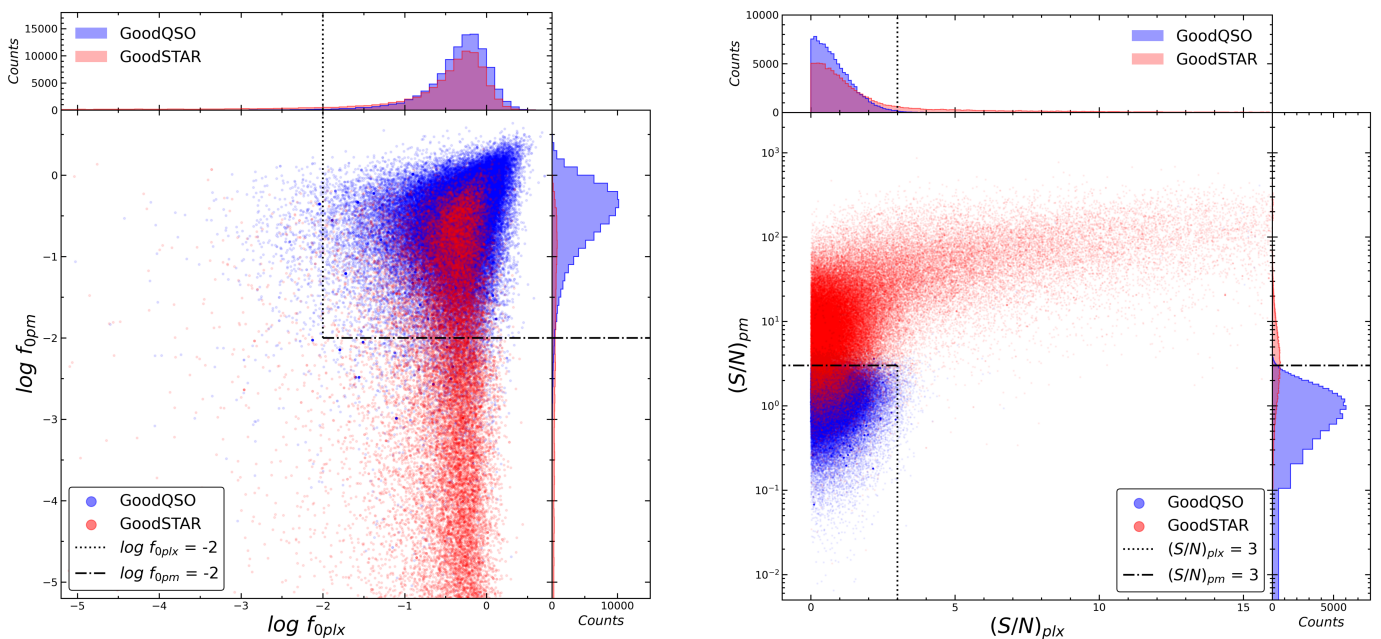


**Fig. 2.** The comparison of the GoodQSO and GoodSTAR distribution in the parameter space of the probability-based method (*left panel*) and the SNR-based method (*right panel*), along with the selection region of the adopted astrometric criteria. The blue and red dots represent the GoodQSO and GoodSTAR, respectively. The black dotted dashed lines represent the probability-based and SNR-based proper motion criteria, respectively. The dotted ones represent the probability-based and SNR-based parallax criteria, respectively. To exhibit the intensive data region and these criteria, both panels display only small parts of the whole distributions.

**Table 1.** Description of the primary columns in the MGQPC catalog.

Column(s)	Description	Example value (unit)
SystemName	The pair name designated by the center coordinates	J000004.061-041259.407
DR3Name_A, DR3Name_B	Unique <i>Gaia</i> DR3 identifier	<i>Gaia</i> DR3 2447741272610542720
RA_A, RA_B	Right ascension (J2000.0)	0.018109143 (degree)
DEC_A, DEC_B	Declination (J2000.0)	-4.215430503 (degree)
Z_A	Redshift of the known quasar	1.851395
Plx_SNR_A, Plx_SNR_B	SNR of parallax	0.298180084
f_0plx_A, f_0plx_B	Probability density of zero parallax	0.30326271
PM_SNR_A, PM_SNR_B	SNR of proper motion	0.962296248
f_0pm_A, f_0pm_B	Probability density of zero proper motion	0.281939962
Gmag_A, Gmag_B	<i>Gaia</i> G-band magnitude	20.251522 (mag)
BPmag_A, BPmag_B	<i>Gaia</i> BP-band magnitude	20.33695 (mag)
RPmag_A, RPmag_B	<i>Gaia</i> RP-band magnitude	19.96667 (mag)
sep_AB	Angular separation between the two members in the pair	11.448785 (")
seplim	Cross-matching radius	11.86317799 (")

**Notes:** The columns with suffix “\_A” describe the known quasar, while those with suffix “\_B” describe the nearby quasar candidate. The last entry “seplim” represents the separation corresponding to a transverse distance of 100 kpc at the known quasar redshift (See Sec. 2.2.1 for details).

in Dawes23, He23, and Wu24, respectively. In Dawes23, 830 individual sources have *Gaia* G-band magnitudes, and 199 systems have at least one member with spectroscopic redshifts. For He23, 1,369 individual sources have *Gaia* G-band magnitudes, and 348 candidate pairs have at least one member with spectroscopic redshifts. And for Wu24, all the candidates have *Gaia* G-band magnitudes, and 1,569 candidates have spectroscopic or photometric redshifts.

Comparative histograms of member separation, *Gaia* G-band magnitude, and redshift distributions are presented in Figure 8 for the three catalogs versus the MGQPCs. In terms of separation distribution (*top panel*), the Dawes23, He23, and

MGQPCs cover ranges of  $0.50'' \sim 4.99''$ ,  $0.51'' \sim 13.93''$ , and  $0.66'' \sim 17.99''$ , respectively. The median separations of the three catalogs are  $1.93''$ ,  $2.04''$ , and  $8.81''$ , respectively. It should be noted that the separation distribution of Wu24 falls within *Gaia*’s resolution range for detecting multi-peak sources ( $0.15'' \sim 0.80''$ ), making its exact distribution and median value uncertain, and its distribution is not plotted in the histogram. The substantial difference in separation distribution and the higher median value of the MGQPC catalog suggest it is more suitable for expanding the quasar pair sample to larger separations, especially in the  $5'' \sim 18''$  range. For the magnitude distribution (*middle panel*), the Dawes23, He23, Wu24, and MGQPCs cover

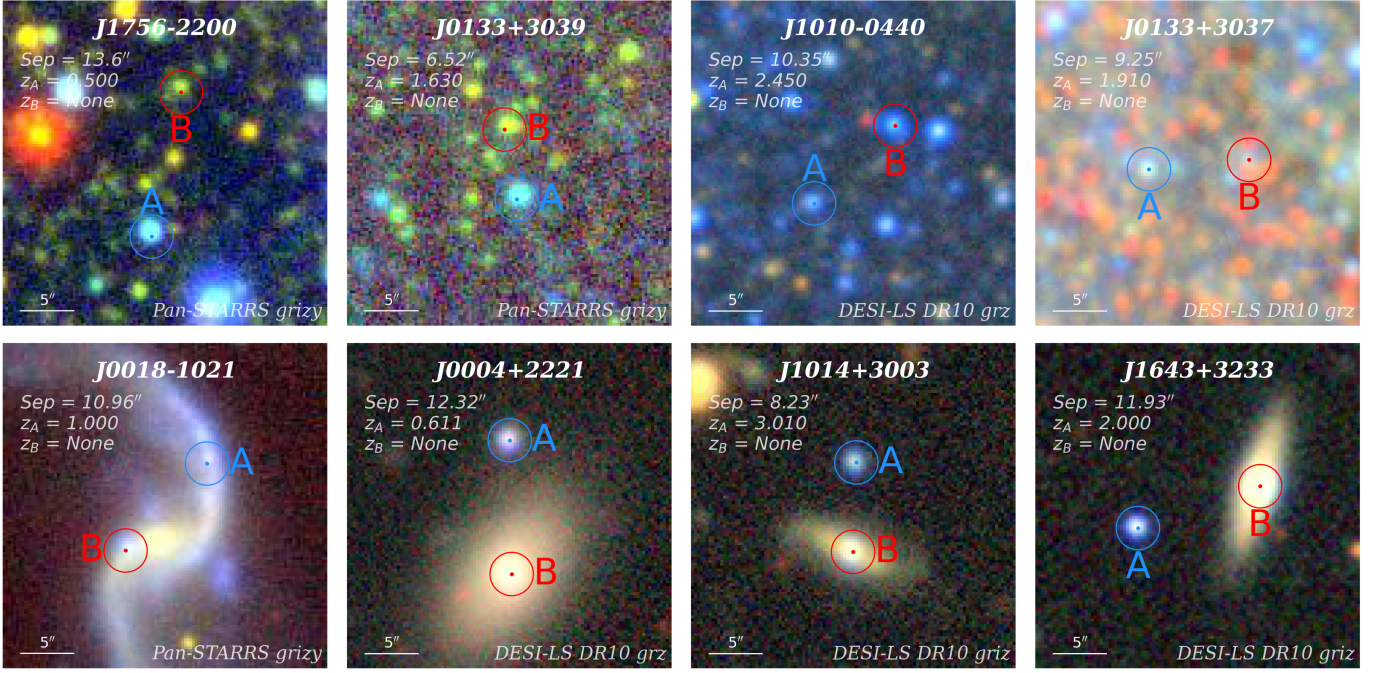


**Fig. 3.** Examples of visually rejected dense stellar fields (*top row*) and nearby galaxies (*bottom row*). The first two pseudo-color images at the *top row* and the first image at the *bottom row* are from Pan-STARRS, and the rest are from the DESI-LS DR10. The blue and red circles with center points mark the quasars from MQCv8 and the astrometrically selected extragalactic candidates in this work, respectively. Their redshifts are denoted by “ $z_A$ ” and “ $z_B$ ”, and the separation between them is denoted by “Sep”. All of these sources are unlikely quasar pairs and were removed. The size of each image is  $30'' \times 30''$  and the north is up while the east is left.

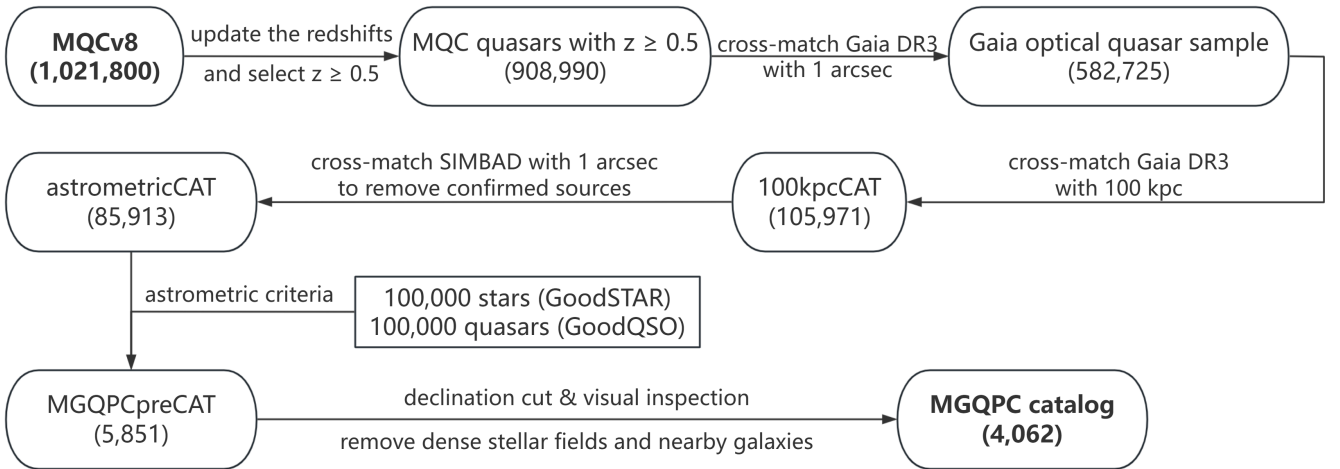


**Fig. 4.** Flowchart of the MGQPC catalog selection process.

16.15 ~ 21.60, 16.34 ~ 21.87, 14.96 ~ 20.50, and 13.46 ~ 21.33, respectively. Their median values are 20.12, 20.02, 19.66, and 20.49, indicating that the MGQPC catalog is slightly fainter and deeper than the other three catalogs. Finally, for the redshift distribution (*bottom panel*), the four catalogs cover 0.29 ~ 3.79, 0 ~ 3.80, 0 ~ 6.11, and 0.50 ~ 6.92, respectively. Their distribution characteristics are generally similar, and the median values are 1.67, 1.71, 1.25, and 1.59, respectively. However, there are still subtle differences: Dawes23 and He23 show higher fractions at  $z \sim 1.5 - 2.5$  than Wu24 and the MGQPC catalog, while Wu24

exhibits a significantly larger fraction at  $z \lesssim 0.5$  compared to the others. Furthermore, the MGQPC catalog shows marginally higher fractions at  $z \sim 0.5 - 1.5$  relative to the three catalogs. Moreover, compared to Wu24, which is a dedicated dual quasar catalog, the MGQPC catalog contains significantly more sources at  $z \sim 0.5 - 2.5$ . This suggests the MGQPC catalog might substantially augment more quasar pairs since the “Cosmic noon” epoch (e.g., Shen et al. 2023b; Chen et al. 2023a; Gross et al. 2024).

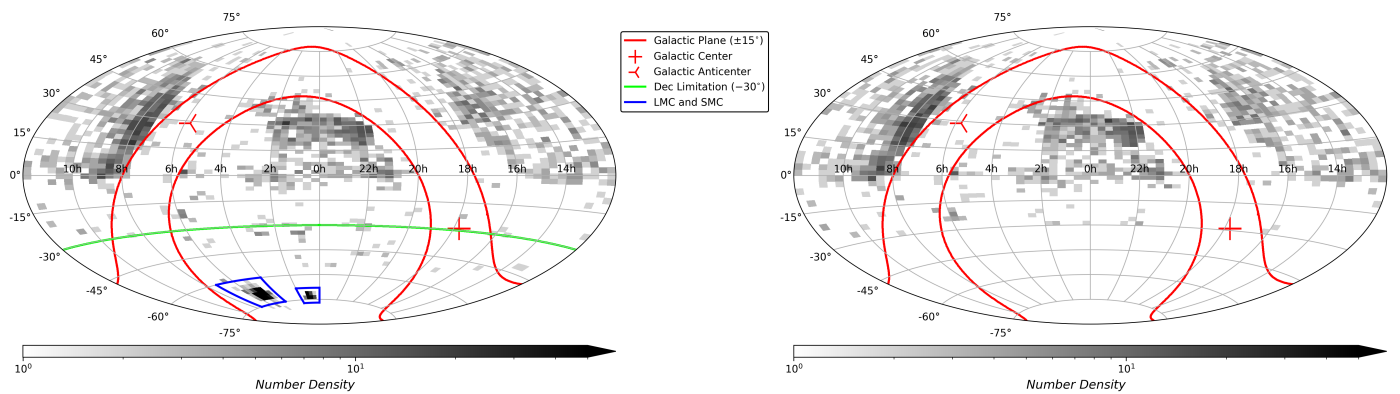


**Fig. 5.** The Hammer-Aitoff projection of the MGQPCpreCAT (*left panel*) and the visually selected MGQPCs (*right panel*). On both panels, the red lines roughly demarcate the Galactic plane ( $|b| \leq 15^\circ$ ), while the red cross and Y-shaped point mark the Galactic center and anti-center, respectively. The coverages of the Large and Small Magellanic Clouds are bounded by the blue quadrilaterals on the *left panel*. A constraint of  $\text{Dec} \geq -30^\circ$  (light green line on the *left panel*) was used to cut out quasar pair candidates for STAGE-I visual inspection and spectroscopic follow-up.

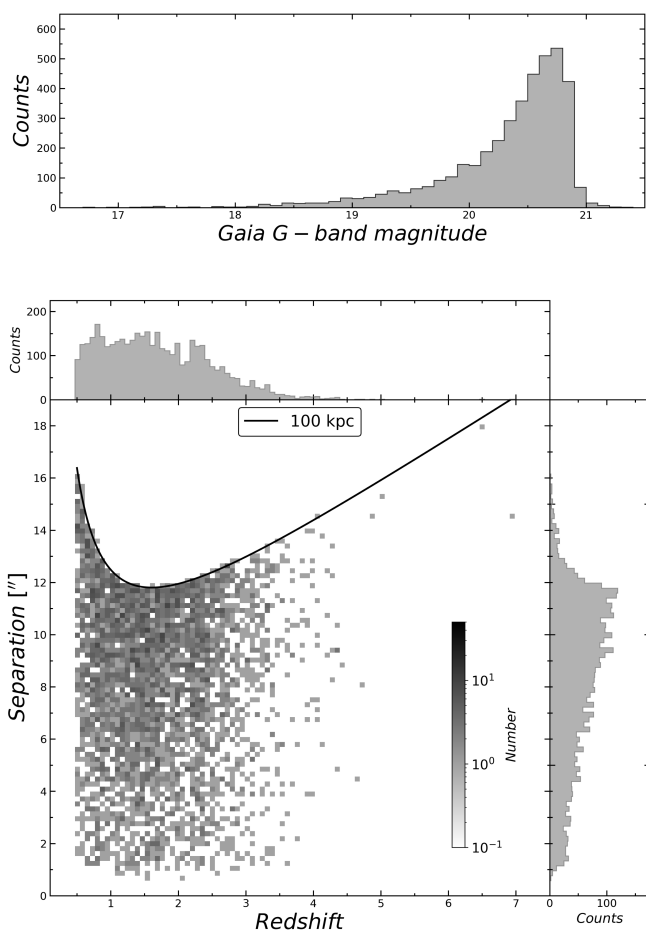


**Fig. 6.** *Top panel:* *Gaia* G-band magnitude histogram of the MGQPCs. *Bottom panel:* separation v.s. redshift (the known quasar) of the MGQPCs. The solid line represents the 100 kpc criterion mentioned in Sec.2.2.1.

On the other hand, the MGQPCs were cross-matched with the three catalogs, yielding 61 matches in Dawes23, 88 in He23, and 5 in Wu24. After excluding these matched candidates (totaling 98 candidate systems), 3,964 new candidates not contained in Dawes23, He23, or Wu24 were obtained. This demonstrates

that the MGQPCs significantly complement existing major candidate quasar pair catalogs, particularly in terms of member separation coverage.

### 3.3. Interesting candidates

The search for quasar pairs inevitably leads to the discovery of lensed quasars, and vice versa (e.g., [Agnello et al. 2018](#); [Lemon et al. 2023](#); [Yue et al. 2023](#); [Dawes et al. 2023](#); [Makarov & Secrest 2023](#); [Ji et al. 2023b, 2024](#)). Currently, most confirmed lensed quasars have small separations, with the majority being within  $4''$ . However, several wide-separation lensed quasars (WSLQs, e.g., [Inada et al. 2003](#); [Shu et al. 2018](#); [Martinez et al. 2023](#); [Napier et al. 2023](#)) have also been discovered. These are typically the result of quasars being lensed by nearby galaxy groups or clusters. WSLQs can also occur when quasars are lensed by single galaxies, producing relatively large separations ranging from  $\sim 6''$  to  $10''$ . The largest separation of a WSLQ lensed by a single massive galaxy discovered to date is  $\sim 10.1''$  (J1651-0417 or “Dragon Kite”, [Ducourant et al. 2019](#); [Stern et al. 2021](#); [Connor et al. 2022](#)).

During the visual inspection, some quasar pair candidates were noted. Their relatively large separation, similar color, and configuration indicate the possibility of being potential WSLQs. These WSLQ candidates exhibit separations from  $\sim 6''$  to  $10''$ , with a potential galaxy located between them. Figure 9 displays three of these potential WSLQs. For a comparison, the unique WSLQ lensed by a single massive galaxy, J1651-0417, is also displayed in Figure 9. Their multi-band photometric data were retrieved from VizieR database<sup>7</sup>, which can be considered ultra-low-resolution spectra (photometric spectra). Multi-epoch measurements of the same band (if any) are averaged to characterize the photometry of that band.

The photometric spectra of the candidate quasars are highly similar to those of known quasars paired with them. This would indicate similar redshifts and spectral features like continuum and/or broad emission lines. Together with the existence of possible foreground galaxies, these systems might be WSLQs lensed by massive galaxies. However, they may also be quasar-galaxy-quasar projection systems, which are precious natural laboratories of detailed study on the circumgalactic medium (e.g., [Krishnarao et al. 2022](#)).

<sup>7</sup> <https://vizier.cds.unistra.fr/viz-bin/VizieR>

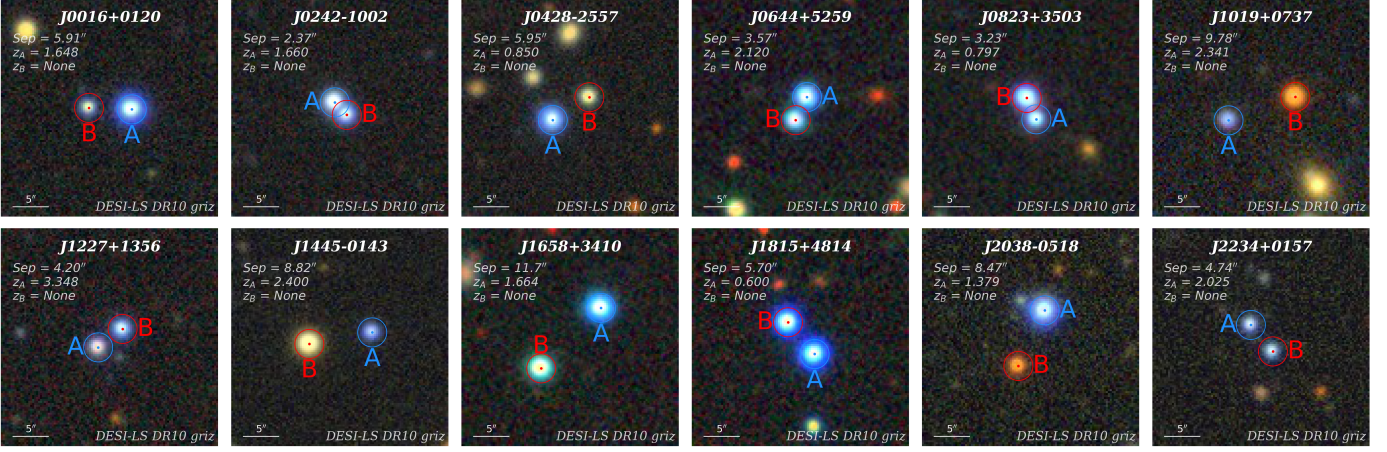


**Fig. 7.** Examples of MGQPCs. All these pseudo-color images are from the DESI-LS DR10. The marks of blue and red circles, image size, direction, and text annotations are the same as in Figure 3.

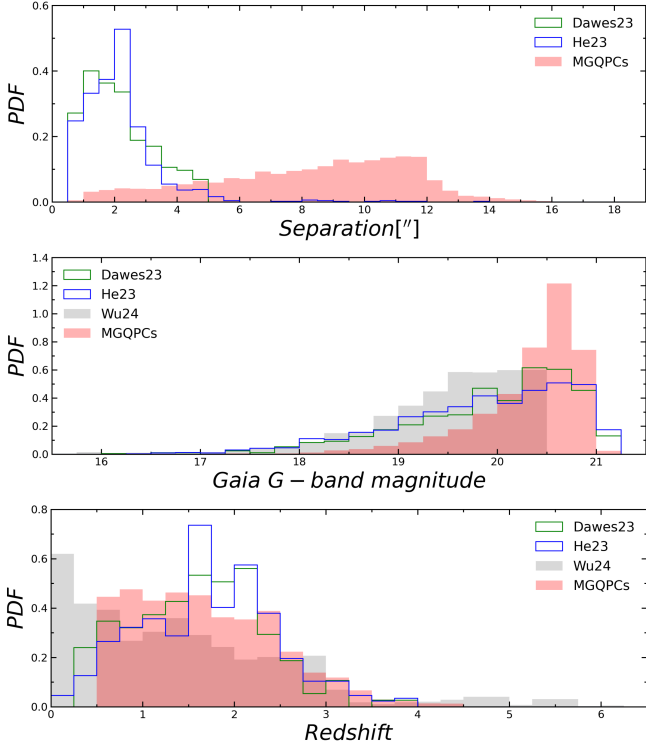


**Fig. 8.** Comparison of Dawes23 (green filled), He23 (blue filled), Wu24 (gray filled), and the MGQPC catalog (red filled) on the distribution of the member separation, *Gaia* G-band magnitude, and redshift. The y-axes are all scaled as probability distribution functions (PDF) to exhibit the distribution characteristics of the three parameters intuitively. *Top panel:* separation histograms of Dawes23, He23, and the MGQPC catalog. *Middle panel:* *Gaia* G-band magnitude histograms of the four catalogs. *Bottom panel:* redshift histograms of the four catalogs.

#### 4. Conclusion and Discussion

This work utilized the current largest quasar catalog, the "Million Quasar Catalog", cross matched it with *Gaia* DR3 to systematically search for quasar pair candidates. The cross-matching radii were determined by a transverse distance of 100

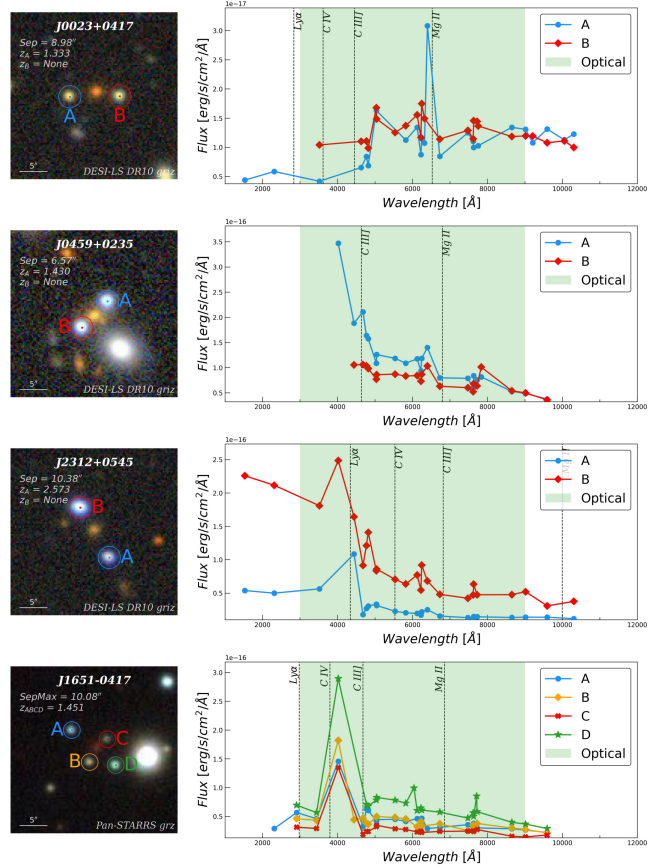


**Fig. 9.** Three potential WSLQs or quasar-galaxy-quasar projection systems noticed during the visual inspection, as well as the J1651-0417. Their photometric spectra show the similarity between the members in each pair system, with several typical emission lines of the known quasars (black dashed lines with line names) and an optical wavelength region of 3000Å ~ 9000Å (green shaded area) overlapping on the photometric spectra. The marks and text annotations in the first three pseudo-color images are the same as in Figure 3 and Figure 7, while the four colored circles, "SepMax", and " $z_{ABCD}$ " denote the quadruply lensed quasars, the largest separation in the J1651-0417 (occurs between A and D), and the redshift of this lensed quasar, respectively.

kpc at the updated redshifts of the known quasars. Based on the reference samples of spectroscopically confirmed quasars and stars of SDSS DR18, a couple of probability-based astrometric criteria were applied to isolate 5,851 extragalactic candidates. Visual inspection was performed on candidates with  $\text{Dec} \geq -30^\circ$  to remove dense stellar fields of the Galactic plane and nearby galaxies. This resulted in 4,062 candidates, which we designated as MGQPCs. The median member separation, *Gaia* G-band magnitude, and redshift of the MGQPCs are 8.81", 20.49, and 1.59, respectively. The MGQPC catalog was compared with three major candidate quasar pair catalogs (Dawes23, He23, and Wu24) to demonstrate its advantages and complementary roles in constructing the quasar pair population. After excluding 98 duplicates shared with the three catalogs, 3,964 previously uncataloged candidates were identified. Some WSLQ candidates were picked out during visual inspection and are briefly described. In recent years, the spectroscopic follow-up using Xinglong 2.16m, Lijiang 2.4m, Palomar 200-inch telescope (P200), and LAMOST was conducted for several tens of MGQPCs. The details of their observation and identification will be reported in the next article.

Although astrometric methods have been proven to be efficient in quasar searches in many studies, the search for quasar pairs not only requires the characteristic of zero proper motion and zero parallax, but also requires that the redshifts of the two member quasars be nearly identical. Therefore, more stringent criteria are still needed to refine the MGQPC catalog. To improve the success rate, several techniques may help:

- Estimating the photometric redshifts of the quasar candidates and selecting those with photometric redshifts similar to the spectroscopic redshifts of the nearby known quasars would be effective in selecting some high-confidence quasar pair candidates.
- Avoiding sky coverages with small stellar proper motions could make sense when searching for quasar candidates with astrometric criteria, as this can make quasars more distinguishable from stars and reduce the stellar contamination. In addition, avoiding sky coverages with dense stellar fields, such as the Galactic plane and the Large and Small Magellanic Clouds, and focusing on high Galactic latitude and the Galactic anti-center areas to search for quasar pair candidates (e.g., Heintz et al. 2015) can also reduce contamination from stars.
- Comparing the photometric spectra or SEDs of the quasar candidates with those of the paired known quasars and selecting those pairs with high similarity in photometric spectra or SEDs as high-probability quasar pair candidates would also work. Note that not all of their photometry across different bands was measured simultaneously, which would result in inaccurate photometric spectra or SEDs. As a reference, and considering that the general variability of quasars is unlikely to change the features of their photometric spectra or SEDs significantly, these photometric data can still be regarded as plausible and useful.
- In the color-based quasar selection, some quasars lying just outside the selection boundaries may be omitted. These quasars with slightly anomalous colors can be easily isolated through astrometric methods (several newly discovered quasars lying just outside the boundaries will be reported in a forthcoming paper). Thus, using the astrometric method would be an effective quasar selection method to isolate sources that are near but outside the quasar selection boundaries.
- Due to the limited fiber diameter of existing surveys, such as the SDSS, LAMOST, and DESI surveys, those quasar pairs or lensed quasars with small separations ( $\lesssim 3''$ ) cannot be resolved spatially and may be identified as single quasars. Therefore, those candidates with very small member separations can be set as high-priority candidates.

Last but not least, visual inspection can only remove nearby galaxies with apparent morphological characteristics, while removing high-redshift or morphologically uncharacteristic galaxies is difficult. Therefore, referencing the morphological classification from *Gaia* or using other classification methods to exclude galaxies is needed to refine the quasar pair candidates.

## Data Availability

The MGQPC catalog is available by contacting the authors via email. Additionally, collaborative opportunities are open to conduct spectroscopic follow-up observations of the MGQPCs.

## Acknowledgments

The authors thank the anonymous referee for the valuable comments that improved the quality and clarity of the manuscript. The authors thank Qirong Yuan, Heng Yu, He Gao, Yiping Shu, Xikai Shan, Yuming Fu, and Yuanzhen Han for their suggestions and guidance on several details. This work has been supported by the Chinese National Natural Science Foundation grant No. 12333001 and by the National Key R&D Program of China (2021YFA0718500).

This work has made use of data from the European Space Agency (ESA) mission *Gaia* (<https://www.cosmos.esa.int/gaia>), processed by the *Gaia* Data Processing and Analysis Consortium (DPAC, <https://www.cosmos.esa.int/web/gaia/dpac/consortium>). Funding for the DPAC has been provided by national institutions, in particular the institutions participating in the *Gaia* Multilateral Agreement.

Funding for the Sloan Digital Sky Survey V has been provided by the Alfred P. Sloan Foundation, the Heising-Simons Foundation, the National Science Foundation, and the Participating Institutions. SDSS acknowledges support and resources from the Center for High-Performance Computing at the University of Utah. SDSS telescopes are located at Apache Point Observatory, funded by the Astrophysical Research Consortium and operated by New Mexico State University, and at Las Campanas Observatory, operated by the Carnegie Institution for Science. The SDSS web site is [www.sdss.org](http://www.sdss.org).

The DESI Legacy Imaging Surveys consist of three individual and complementary projects: the Dark Energy Camera Legacy Survey (DECaLS), the Beijing-Arizona Sky Survey (BASS), and the Mayall z-band Legacy Survey (MzLS). Pipeline processing and analyses of the data were supported by NOIRLab and the Lawrence Berkeley National Laboratory (LBNL). Legacy Surveys was supported by: the Director, Office of Science, Office of High Energy Physics of the U.S. Department of Energy; the National Energy Research Scientific Computing Center, a DOE Office of Science User Facility; the U.S. National Science Foundation, Division of Astronomical Sciences; the National Astronomical Observatories of China, the Chinese Academy of Sciences and the Chinese National Natural Science Foundation. LBNL is managed by the Regents of the University of California under contract to the U.S. Department of Energy.

The Pan-STARRS1 Surveys (PS1) and the PS1 public science archive have been made possible through contributions by

the Institute for Astronomy, the University of Hawaii, the Pan-STARRS Project Office, the Max-Planck Society and its participating institutes, the Max Planck Institute for Astronomy, Heidelberg and the Max Planck Institute for Extraterrestrial Physics, Garching, The Johns Hopkins University, Durham University, the University of Edinburgh, the Queen's University Belfast, the Harvard-Smithsonian Center for Astrophysics, the Las Cumbres Observatory Global Telescope Network Incorporated, the National Central University of Taiwan, the Space Telescope Science Institute, the National Aeronautics and Space Administration under Grant No. NNX08AR22G issued through the Planetary Science Division of the NASA Science Mission Directorate, the National Science Foundation Grant No. AST-1238877, the University of Maryland, Eotvos Lorand University (ELTE), the Los Alamos National Laboratory, and the Gordon and Betty Moore Foundation.

We acknowledge the use of public data from the following facilities: *Gaia*, SDSS, DESI Legacy Survey, Pan-STARRS. This research made use of the following software packages: Astropy (Astropy Collaboration et al. 2013, 2018, 2022), Matplotlib (Hunter 2007), NumPy (van der Walt et al. 2011; Harris et al. 2020), Pandas (Wes McKinney 2010; pandas development team 2022), TOPCAT (Taylor 2005).

## References

- Agnello, A., Schechter, P. L., Morgan, N. D., et al. 2018, MNRAS, 475, 2086  
 Altamura, E., Brennan, S., Leśniewska, A., et al. 2020, AJ, 159, 122  
 An, T., Zhang, Y., Wang, A., et al. 2022, A&A, 663, A139  
 Antonucci, R. 1993, ARA&A, 31, 473  
 Astropy Collaboration, Price-Whelan, A. M., Lim, P. L., et al. 2022, ApJ, 935, 167  
 Astropy Collaboration, Price-Whelan, A. M., Sipőcz, B. M., et al. 2018, AJ, 156, 123  
 Astropy Collaboration, Robitaille, T. P., Tollerud, E. J., et al. 2013, A&A, 558, A33  
 Begelman, M. C., Blandford, R. D., & Rees, M. J. 1980, Nature, 287, 307  
 Bolton, J. G., Peterson, B. A., Wills, B. J., & Wills, D. 1976, ApJ, 210, L1  
 Boroson, T. A. & Lauer, T. R. 2009, Nature, 458, 53  
 Bromley, B. C., Sandick, P., & Shams Es Haghi, B. 2024, Phys. Rev. D, 110, 023517  
 Chambers, K. C., Magnier, E. A., Metcalfe, N., et al. 2016, arXiv e-prints, arXiv:1612.05560  
 Charisi, M., Bartos, I., Haiman, Z., et al. 2016, MNRAS, 463, 2145  
 Chen, Y., Yu, Q., & Lu, Y. 2020, ApJ, 897, 86  
 Chen, Y.-C. 2021, arXiv e-prints, arXiv:2109.06881  
 Chen, Y.-C., Hwang, H.-C., Shen, Y., et al. 2022, ApJ, 925, 162  
 Chen, Y.-C., Liu, X., Foord, A., et al. 2023a, Nature, 616, 45  
 Chen, Y.-C., Liu, X., Lazio, J., et al. 2023b, ApJ, 958, 29  
 Ciurlo, A., Mannucci, F., Yeh, S., et al. 2023, A&A, 671, L4  
 Connor, T., Stern, D., Krone-Martins, A., et al. 2022, ApJ, 927, 45  
 Davis, M. C., Grace, K. E., Trump, J. R., et al. 2024, ApJ, 965, 34  
 Dawes, C., Storfer, C., Huang, X., et al. 2023, ApJS, 269, 61  
 de Bruijne, J. H. J. 2012, Ap&SS, 341, 31  
 De Rosa, A., Vignali, C., Bogdanović, T., et al. 2019, New A Rev., 86, 101525  
 DESI Collaboration, Abdul-Karim, M., Adame, A. G., et al. 2025, arXiv e-prints, arXiv:2503.14745  
 Dey, A., Schlegel, D. J., Lang, D., et al. 2019, AJ, 157, 168  
 Djorgovski, S., Perley, R., Meylan, G., & McCarthy, P. 1987, ApJ, 321, L17  
 Du, P. & Wang, J.-M. 2023, A&A, 671, A26  
 Ducourant, C., Krone-Martins, A., Delchambre, L., et al. 2019, in SF2A-2019: Proceedings of the Annual meeting of the French Society of Astronomy and Astrophysics, ed. P. Di Matteo, O. Creevey, A. Crida, G. Kordopatis, J. Malzac, J. B. Marquette, M. N'Diaye, & O. Venot, Di  
 Eracleous, M., Boroson, T. A., Halpern, J. P., & Liu, J. 2012a, ApJS, 201, 23  
 Eracleous, M., Flohic, H. M. L. G., & Bogdanović, T. 2012b, in Astronomical Society of the Pacific Conference Series, Vol. 460, AGN Winds in Charleston, ed. G. Chartas, F. Hamann, & K. M. Leighly, 214  
 Eracleous, M., Halpern, J. P., M. Gilbert, A., Newman, J. A., & Filippenko, A. V. 1997, ApJ, 490, 216  
 Fleisch, E. W. 2015, PASA, 32, e010  
 Fleisch, E. W. 2023, The Open Journal of Astrophysics, 6, 49  
 Foord, A., Gültekin, K., Nevin, R., et al. 2020, ApJ, 892, 29  
 Fu, Y., Wu, X.-B., Yang, Q., et al. 2021, ApJS, 254, 6  
 Gaia Collaboration, Prusti, T., de Bruijne, J. H. J., et al. 2016, A&A, 595, A1  
 Gaia Collaboration, Vallenari, A., Brown, A. G. A., et al. 2022, arXiv e-prints, arXiv:2208.00211  
 Graham, M. J., Djorgovski, S. G., Stern, D., et al. 2015a, MNRAS, 453, 1562  
 Graham, M. J., Djorgovski, S. G., Stern, D., et al. 2015b, Nature, 518, 74  
 Green, P. J., Myers, A. D., Barkhouse, W. A., et al. 2010, ApJ, 710, 1578  
 Gross, A. C., Chen, Y.-C., Oguri, M., et al. 2024, arXiv e-prints, arXiv:2409.16363  
 Guo, H., Liu, X., Shen, Y., et al. 2019, MNRAS, 482, 3288  
 Harris, C. R., Millman, K. J., van der Walt, S. J., et al. 2020, Nature, 585, 357  
 He, Z., Chen, Q., Deng, L., et al. 2025, A&A, 695, A76  
 He, Z., Li, N., Cao, X., et al. 2023, A&A, 672, A123  
 Heintz, K. E., Fynbo, J. P. U., Geier, S. J., et al. 2020, A&A, 644, A17  
 Heintz, K. E., Fynbo, J. P. U., & Høg, E. 2015, A&A, 578, A91  
 Heintz, K. E., Fynbo, J. P. U., Høg, E., et al. 2018, A&A, 615, L8  
 Hennawi, J. F., Myers, A. D., Shen, Y., et al. 2010, ApJ, 719, 1672  
 Hennawi, J. F., Strauss, M. A., Oguri, M., et al. 2006, AJ, 131, 1  
 Hou, M., Li, Z., & Liu, X. 2020, ApJ, 900, 79  
 Hunter, J. D. 2007, Computing in Science and Engineering, 9, 90  
 Hwang, H.-C., Shen, Y., Zakamska, N., & Liu, X. 2020, ApJ, 888, 73  
 Impey, C. 1998, in Astronomical Society of the Pacific Conference Series, Vol. 146, The Young Universe: Galaxy Formation and Evolution at Intermediate and High Redshift, ed. S. D'Odorico, A. Fontana, & E. Giallongo, 391  
 Inada, N., Oguri, M., Pindor, B., et al. 2003, Nature, 426, 810  
 Ji, X., Zheng, Z.-Y., Lin, R.-Q., & Feng, H.-C. 2024, arXiv e-prints, arXiv:2412.08397  
 Ji, X., Zheng, Z.-Y., Wu, Q., et al. 2023a, MNRAS, 524, 1909  
 Ji, X., Zheng, Z.-Y., Wu, Q., et al. 2023b, MNRAS, 524, 1909  
 Kelley, L., Charisi, M., Burke-Spolaor, S., et al. 2019, BAAS, 51, 490  
 Kim, D., Im, M., Kim, M., & Ho, L. C. 2020a, ApJ, 894, 126  
 Kim, D. C., Yoon, I., Evans, A. S., et al. 2020b, ApJ, 904, 23  
 Komossa, S., Burwitz, V., Hasinger, G., et al. 2003, ApJ, 582, L15  
 Koo, D. C., Kron, R. G., & Cudworth, K. M. 1986, PASP, 98, 285  
 Koo, H., Bak, D., Park, I., Hong, S. E., & Lee, J.-W. 2024, Physics Letters B, 856, 138908  
 Krishnarao, D., Fox, A. J., D'Onghia, E., et al. 2022, Nature, 609, 915  
 Lemon, C., Anguita, T., Auger-Williams, M. W., et al. 2023, MNRAS, 520, 3305  
 Lemon, C. A., Auger, M. W., & McMahon, R. G. 2019, MNRAS, 483, 4242  
 Lemon, C. A., Auger, M. W., McMahon, R. G., & Kaposov, S. E. 2017, MNRAS, 472, 5023  
 Liao, W.-T., Chen, Y.-C., Liu, X., et al. 2021, MNRAS, 500, 4025  
 Liu, F. K., Wu, X.-B., & Cao, S. L. 2003, MNRAS, 340, 411  
 Liu, X., Shen, Y., Strauss, M. A., & Hao, L. 2011, ApJ, 737, 101  
 Liu, Y. 2015, A&A, 580, A133  
 Liu, Y. 2016, A&A, 592, L4  
 Makarov, V., Bergeha, C., Boboltz, D., et al. 2012, Mem. Soc. Astron. Italiana, 83, 952  
 Makarov, V. V. & Secrest, N. J. 2022, ApJ, 933, 28  
 Makarov, V. V. & Secrest, N. J. 2023, ApJS, 264, 4  
 Mannucci, F., Pancino, E., Belfiore, F., et al. 2022, Nature Astronomy, 6, 1185  
 Mannucci, F., Scialpi, M., Ciurlo, A., et al. 2023, A&A, 680, A53  
 Martínez, M. N., Napier, K. A., Cloonan, A. P., et al. 2023, ApJ, 946, 63  
 Merritt, D. 2013, Dynamics and Evolution of Galactic Nuclei  
 Merritt, D. & Milosavljević, M. 2005, Living Reviews in Relativity, 8, 8  
 Meylan, G., Djorgovski, S., Perley, R., & McCarthy, P. 1987, The Messenger, 48, 34  
 Milosavljević, M. & Merritt, D. 2001, ApJ, 563, 34  
 Muñoz, J. A., Falco, E. E., Kochanek, C. S., et al. 1998, ApJ, 492, L9  
 Myers, A. D., Richards, G. T., Brunner, R. J., et al. 2008, ApJ, 678, 635  
 Napier, K., Gladders, M. D., Sharon, K., et al. 2023, ApJ, 954, L38  
 Netzer, H. 2015, ARA&A, 53, 365  
 pandas development team, T. 2022, pandas-dev/pandas: Pandas, if you use this software, please cite it as below.  
 Pfeifle, R. W., Weaver, K. A., Secrest, N. J., Rothberg, B., & Patton, D. R. 2024, arXiv e-prints, arXiv:2411.12799  
 Ross, N. P., Myers, A. D., Sheldon, E. S., et al. 2012, ApJS, 199, 3  
 Sandage, A. 1965, ApJ, 141, 1560  
 Sandrinelli, A., Falomo, R., Treves, A., Farina, E. P., & Uslenghi, M. 2014, MNRAS, 444, 1835  
 Sandrinelli, A., Falomo, R., Treves, A., Scarpa, R., & Uslenghi, M. 2018, MNRAS, 474, 4925  
 Schmidt, M. 1963, Nature, 197, 1040  
 Schwartzman, E., Clarke, T. E., Nyland, K., et al. 2024, ApJ, 961, 233  
 Scialpi, M., Mannucci, F., Marconcini, C., et al. 2024, A&A, 690, A57  
 Shen, Y., Casey-Clyde, J. A., Chen, Y.-C., et al. 2023a, arXiv e-prints, arXiv:2306.15527  
 Shen, Y., Chen, Y.-C., Hwang, H.-C., et al. 2021, Nature Astronomy, 5, 569  
 Shen, Y., Hennawi, J. F., Shankar, F., et al. 2010, ApJ, 719, 1693  
 Shen, Y., Hwang, H.-C., Oguri, M., et al. 2023b, ApJ, 943, 38

- Shen, Y., Hwang, H.-C., Zakamska, N., & Liu, X. 2019, *ApJ*, 885, L4
- Shen, Y. & Loeb, A. 2010, *ApJ*, 725, 249
- Shu, Y., Kuposov, S. E., Evans, N. W., et al. 2019, *MNRAS*, 489, 4741
- Shu, Y., Marques-Chaves, R., Evans, N. W., & Pérez-Fournon, I. 2018, *MNRAS*, 481, L136
- Sillanpää, A., Haarala, S., Valtonen, M. J., Sundelius, B., & Byrd, G. G. 1988, *ApJ*, 325, 628
- Silverman, J. D., Tang, S., Lee, K.-G., et al. 2020, *ApJ*, 899, 154
- Souchay, J., Secrest, N., Lambert, S., et al. 2022, *A&A*, 660, A16
- Stern, D., Djorgovski, S. G., Krone-Martins, A., et al. 2021, *ApJ*, 921, 42
- Stockton, A. N. 1972, *Nature Physical Science*, 238, 37
- Tang, S. & Grindlay, J. 2009, *ApJ*, 704, 1189
- Tang, S., Silverman, J. D., Ding, X., et al. 2021, arXiv e-prints, arXiv:2105.10163
- Taylor, M. B. 2005, in *Astronomical Society of the Pacific Conference Series*, Vol. 347, *Astronomical Data Analysis Software and Systems XIV*, ed. P. Shopbell, M. Britton, & R. Ebert, 29
- Uppal, A., Ward, C., Gezari, S., et al. 2024, arXiv e-prints, arXiv:2405.11026
- Urry, C. M. & Padovani, P. 1995, *PASP*, 107, 803
- van der Walt, S., Colbert, S. C., & Varoquaux, G. 2011, *Computing in Science and Engineering*, 13, 22
- Wampler, E. J., Baldwin, J. A., Burke, W. L., & Robinson, L. B. 1973, *Nature*, 246, 203
- Wang, H.-C., Wang, J.-X., Gu, M.-F., & Liao, M. 2023a, *MNRAS*, 524, L38
- Wang, J.-M., Songsheng, Y.-Y., Li, Y.-R., & Du, P. 2023b, *MNRAS*, 518, 3397
- Wenger, M., Ochsenein, F., Egret, D., et al. 2000, *A&AS*, 143, 9
- Wes McKinney. 2010, in *Proceedings of the 9th Python in Science Conference*, ed. Stéfan van der Walt & Jarrod Millman, 56 – 61
- Wright, E. L., Eisenhardt, P. R. M., Mainzer, A. K., et al. 2010, *AJ*, 140, 1868
- Wu, Q., Liao, S., Qi, Z., et al. 2023, *Research in Astronomy and Astrophysics*, 23, 025006
- Wu, Q., Scialpi, M., Liao, S., Mannucci, F., & Qi, Z. 2024, *A&A*, 692, A154
- Wu, Q.-Q., Liao, S.-L., Ji, X., et al. 2022, *Frontiers in Astronomy and Space Sciences*, 9, 822768
- Wu, X.-B., Hao, G., Jia, Z., Zhang, Y., & Peng, N. 2012, *AJ*, 144, 49
- Xu, W., Cui, L., Liu, X., et al. 2024, *ApJ*, 969, 36
- Yan, C.-S., Lu, Y., Dai, X., & Yu, Q. 2015, *ApJ*, 809, 117
- Yèche, C., Palanque-Delabrouille, N., Claveau, C.-A., et al. 2020, *Research Notes of the American Astronomical Society*, 4, 179
- York, D. G., Adelman, J., Anderson, John E., J., et al. 2000, *AJ*, 120, 1579
- Yu, Q. 2002, *MNRAS*, 331, 935
- Yue, M., Fan, X., Yang, J., & Wang, F. 2023, *AJ*, 165, 191
- Zhang, F. 2023, arXiv e-prints, arXiv:2312.11847
- Zheng, Q., Liu, S., Zhang, X., & Yuan, Q. 2023, *ApJ*, 944, 4
- Zheng, Q., Zhang, X., Yuan, Q., Severgnini, P., & Vignali, C. 2024, *MNRAS*, 531, L76
- Zhou, H., Wang, T., Zhang, X., Dong, X., & Li, C. 2004, *ApJ*, 604, L33